http://dx.doi.org/10.1016/j.ijepes.2021.000000

# An Impulse Modulation Strategy for the m-Phase Permanent Magnet Synchronous Motor with Current Source Inverter

First Author[a], Second Author[b], Third Author[a,b,*]

[a]*First affiliation, Address, City and Postcode, Country*
[b]*Second affiliation, Address, City and Postcode, Country*

**Abstract**

In order to reduce the complexity of the traditional space vector pulse width modulation (SVPWM) strategy, this paper proposes a novel impulse modulation strategy for the m-phase permanent magnet synchronous motor with current source inverter. This method includes two parts: the current impulse duty calculation and the generation of pulse width modulation (PWM). By using the inverse Park transform and the inverse Clarke transform, the target current impulse duties can be obtained from the control variables of the d-q axis. According to the characteristic that only one upper switch and one lower switch of the current source inverter turns on at any time, the impulse duties can be sorted from large value to small one, the comparison points can be calculated, and then the PWM can be generated from the comparison points. Since the PWM is sorted from large to small values, the final PWM needs to be generated by inverse sorting. At an m-phase motor drive system, the proposed method requires m current impulses to control the system, but the SVPWM needs $m^2$ space current vectors. This method does not select the sector, and the calculation of the comparison points and the generation of the PWM can be achieved without the change of the equations. However, the SVPWM needs to select different space current vectors to calculate the comparison points and generate the PWM by different sectors. Compared to the SVPWM, this method has similar performance in the aspect of the efficiency, output current harmonic, bus current utilization ratio and dynamic response. And this method can be easily extended to multi-phase current source inverter. Experimental results have verified the effectiveness of the proposed method

*Keywords:* Current source inverter; impulse modulation; permanent magnet synchronous motor; space vector pulse width modulation.

## 1. Introduction

Thanks to the advantages of high reliability, low acoustic noise, small size, and lofty torque to inertia [1]-[5], the permanent magnet synchronous motor (PMSM) has been widely used in many applications, such as aerospace, electric vehicles, wind generation systems and electric vehicles [6]-[7]. The driver circuit of PMSM is mainly divided into two types: the voltage source inverter (VSI) and current source inverter (CSI). Thanks to the advantages of four-quadrant operation, motor friendly output phase voltages, inherent short circuit protection, and relatively low electromagnetic interference (EMI) [8]-[10], the CSI has drawn great attention.

At present, the commonly used pulse width modulation (PWM) technologies are the sinusoidal pulse width modulation (SPWM), space vector pulse width modulation (SVPWM), and selective harmonic elimination pulse width modulation (SHEPWM), etc. [11]. Due to the advantage of good dynamic performance [12], the SVPWM has been widely used in PMSM drives. However, there are still many problems with the conventional SVPWM, such as common mode voltage, LC resonance, and calculation complexity.

To reduce the common mode voltage, some modified modulation strategies have been proposed. Y. Xu proposed a modulation strategy without using zero vectors [8], which utilizes the switches in auxiliary power circuit to

* Corresponding author. Tel.: +0-000-000-0000 ; fax: +0-000-000-0000 .
*E-mail address:* author@institute.xxx
http://dx.doi.org/10.1016/j.ijepes.2021.00.000
0142-0615 /

construct the zero current vector for CSI. X. Guo proposed a new common mode voltage mitigation technique [13], which coordinates the active and zero vectors instead of eliminating zero vectors or optimal selection of a zero vector. A. Hu proposed a new space vector modulation-based strategy for high-power CSIs using synthesized reference trajectory on the hexagon on the α-β plane [14], which eliminates the unwanted low-order harmonics by combining the proposed space vector modulation (SVM) with SHEPWM. Since the space vector modulation of the three-leg CSI has the disadvantages of the bipolar current pulses and modulation index range limitation, X. Guo proposed a four-leg CSI with a new space vector modulation [15]. J. Shang investigated three possible zero-state vector selection strategies in the reduced common mode voltage (CMV) space vector modulation for the CSI [16], which can then be considered for different types of drives to reduce the insulation stress or to limit the resonance in the common mode circuit. By allowing the use of zero-state vectors, J. Shang proposed a reduced CMV space-vector modulation method for CSIs [17]. In the case of low motor speeds, Y. Lian proposed a solution based on average-value-reduction space-vector modulation [18]. H. Gao proposed a CMV reduced model-predictive control to further mitigate the CMV peak value through selecting optimal space vectors [19].

In addition, researchers have conducted a lot of research on other issues as well. In order to attenuate the common-mode current, Y. Lian proposed three modified average-value-reduction space vector modulation schemes [20], where the single long zero vector is separated into segments in the PWM sequence. To remove the pre-circuit of the CSI, G. Migliazza proposed an innovative idc current control scheme [9]. To suppress the LC resonance for the high power current-source inverter fed drives, E. Lorenzani proposed a suitable space vector modulation strategy [21], in which the excitation of the LC filter can be attenuated without the use of any passive or active damping solutions. And Z. Wang proposed a hybrid pulse width modulation based on selective harmonic elimination and SVPWM [22]. To modulate the torque with voltage regulator, A. N. Ghule proposed a complex vector voltage regulator control approach as a means for modulating torque [23]. To reduce the dc-link current ripple, P. Liu proposed an optimized space vector modulation strategy [24], X. Guo proposed a new space vector control strategy by dividing the space vector into 12 sectors [25], and a modified space vector modulation by adjusting the gate patterns [26]. Based on the estimation of resonance conditions, Y. Zhang developed a dc-link virtual impedance-based control method [27], which enables the SHE modulated PWM CSR to actively mitigate the significant dc-link current inter-harmonics. To achieve less THD as well as better dynamic performance, G. S. Kulothungan proposed a single modulation technique called optimal SVM technique [12], which can attain low THD of output current, while limiting the device switching frequency to 450 Hz. To achieve lower output total harmonic distortion, W. Wang proposed an eight-switch, five-level current source inverter and the corresponding space-vector-modulation strategy for the proposed CSI topology [28]. Since the overlap time will cause negative influence in the output current waveform, Y. Geng proposed an overlap-time compensation method [29], which compensates the dwell time of vectors according to the relations of voltages. To decrease the weight and size, A. Singh proposed a zero dc-link impedance topology with a phasor pulse-width modulation boost current source inverter [30]. To suppress the leakage current, X. Guo proposed a new three-phase current source H7 inverter and a new space vector modulation [31]. S. Anand proposed a modified CSI with modified space vector modulation without using an isolation transformer [32], which increases the efficiency and reduces the cost as compared to conventional current source.

From the above-mentioned researches, although the CSI PWM technique has been studied a lot, the high complexity of the SVPWM still cannot be solved well. To reduce the complexity of the conventional SVPWM strategy, this paper proposes a novel impulse modulation PWM technique. According to the characteristic that only one upper switch and one lower switch of the current source inverter turns on at any time, the impulse duties can be sorted from large to small values, the comparison points can be calculated, and then the PWM can be generated from the comparison points. Since the PWM is sorted from large to small values, the final PWM needs to be generated by inverse sorting.

The structure of this paper is organized as follows: Section II introduces the proposed impulse modulation strategy, Section III describes the experimental platform, Section IV presents the experimental results and discussions, and Section V concludes the paper.

## 2. Mathematical model

### *2.1. The m-phase current source inverter topology*

As shown in Fig. 1, the *m*-phase current source inverter is composed of two circuits, the pre-stage buck circuit which is used to generate a constant dc-link current $i_{dc}$ and the second-stage, i.e. the *m*-phase current source half-bridge inverter. The load is the *m*-phase permanent magnet synchronous motor (PMSM). $C_1$~$C_m$ are the *m*-phase star connection capacitor filters. And the current source inverter should be connected with the diode in series, as shown in $D_1$~$D_{2m}$.

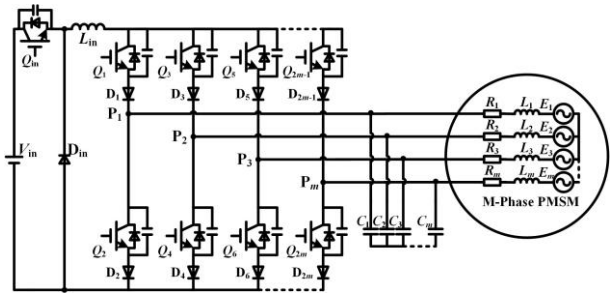


Fig. 1. The topology of the m-phase current source inverter.

### *2.2. Mathematical model of the impulse modulation strategy*

According to the impulse principle, there are *m* current impulses in an *m*-phase PMSM. In the digital control system, each current impulse can be generated by the dc-link current chopper, that is, there is a duty cycle, the PWM can be obtained from the duty cycle, and then the current impulse control can be realized.

Based on the principle of area equivalence, each phase current impulse is

$$i_{k,\mathrm{impulse}} = i_k \times t_s = t_k \times i_{dc}, k \in \{1,2,...,m\}, t_k \in [-t_s, t_s], \tag{1}$$

where $i_{k,\mathrm{impulse}}$ is the current impulse of phase *k*, $i_k$ is the current of phase *k*, $i_{dc}$ is the dc-link current, $t_s$ is the control period, $t_k$ is the conducting time of the switch of phase *k*, and *m* is the number of phases. When $t_k$ is positive, the upper switch of the phase is on, or the lower switch is on.

According to the modulation features of the current source inverter, only one upper switch and one lower switch conduct at any working time. Assume that the duty cycle of phase *k* is

$$D_k = \frac{t_k}{t_s}. \tag{2}$$

Then the current of phase *k* is

$$i_k = D_k \times i_{dc}. \tag{3}$$

And the duty cycle set *D* is

$$D = \{D_1, D_2, ..., D_m\}, \tag{4}$$

where $D_k$ is the duty cycle of phase $k$, $D_k \in [-1,1]$, $k \in \{1, 2, \cdots, m\}$. Since the sum of phase currents should be zero, the sum of phase duty cycles also should be zero, that is

$$\sum_{k=1}^{m} D_k = 0, D_k \in D. \tag{5}$$

Sorting the duty cycle of the set $D$ in order from large to small values, the new duty cycle set $d$ is

$$d = \{d_1, d_2, ..., d_m\}, d_k \in D, k \in \{1, 2, ..., m\}, \tag{6}$$

where $d_i \geqslant d_{i+1}$, $d_i \in d$, $i \in \{1, 2, \cdots, m\text{-}1\}$. The sort mappings can be defined as

$$[d_1, d_2, ..., d_m]^{\mathrm{T}} = A[D_1, D_2, ..., D_m]^{\mathrm{T}}, \tag{7}$$

where $A$ is the square matrix of order $m$, that is

$$A = \begin{bmatrix} A_{11} & \mathrm{L} & A_{1m} \\ \mathrm{M} & \mathrm{O} & \mathrm{M} \\ A_{m1} & \mathrm{L} & A_{mm} \end{bmatrix}, \tag{8}$$

For $A_{i,j}$, $i, j \in \{1, 2, \cdots, m\}$, if

$$d_i = D_j, d_i \in d, D_j \in D, \tag{9}$$

then $A_{i,j} = 1$, otherwise $A_{i,j} = 0$. Since the sum of the phase duty cycles is zero, and the duty cycle of each phase cannot all be zero during normal operation, there must be an integer $n$ which can meet the requirement

$$d_n \geqslant 0, d_{n+1} < 0, n \in \{1, 2, ..., m\text{-}1\}. \tag{10}$$

Then the sum $d_\mathrm{p}$ of the positive duty cycles is

$$d_\mathrm{p} = \sum_{k=1}^{n} d_k, d_k > 0. \tag{11}$$

When $d_\mathrm{p} > 1$, it represents that the system has been in the over-modulation area, and the duty cycle set $d$ should be modified to

$$d' = \left\{ d_k' \middle| d_k' = \frac{d_k}{d_p}, d_k \in d \right\}. \tag{12}$$

Then the duty cycle set $D_\mathrm{g}$ can be obtained as

$$D_{\mathrm{g}} = \begin{cases} d, d_p \le 1 \\ d \notin d_p > 1 \end{cases}. \tag{13}$$

According to the duty cycle set $D_{\mathrm{g}}$, the comparison point set $T_{\mathrm{g}}$ can be further obtained as

$$T_{\mathrm{g}} = \{T_1, T_2, ..., T_n, T_{n+1}, T_{n+2}, ..., T_m\}, \tag{14}$$

and any comparison point $T_k$ is

$$T_k = \begin{cases} \frac{t_0}{4}, t_0 = 1 - \sum_{i=1}^{n} d_i, k = 1 \\ T_{k-1} + \frac{d_{k-1}}{2}, k \in \{2, 3, ..., n\} \\ T_{k+1} + \frac{d_{k+1}}{2}, k \in \{n+1, n+2, ..., m-1\} \\ -\frac{t_0}{4}, t_0 = 1 - \sum_{i=1}^{n} d_i, k = 1 \end{cases}, \tag{15}$$

where $d_i$, $d_{k-1}$, $d_{k+1} \in D_{\mathrm{g}}$, $T_{k-1}$, $T_{k+1} \in T_{\mathrm{g}}$. When generating the PWM waveform, similar to the SVPWM, the carrier adopts unipolar triangular carrier $T_{\mathrm{cmp}}$, and the carrier amplitude is set as 0.5, and the frequency is $f_{\mathrm{s}}$, then the PWM wave set $G$ is

$$G = \{p_1, p_2, ..., p_m\}, \tag{16}$$

where $p_k \in G$, $T_k \in T_{\mathrm{g}}$, $d_k \in D_{\mathrm{g}}$, $k \in \{1, 2, \ldots, m\}$, and $p_k$ is

$$p_k = \begin{cases} 1, T_k \le T_{\mathrm{cmp}} < T_k + \frac{d_k}{2}, d_k > 0 \\ 2, |T_k| \le T_{\mathrm{cmp}} < \left| T_k + \frac{d_k}{2} \right|, d_k < 0 \\ 3, T_{\mathrm{cmp}} < |T_1|, or, T_{\mathrm{cmp}} > \left| T_n + \frac{d_n}{2} \right| \\ 4, T_{\mathrm{cmp}} < |T_k|, k \neq 1, or, T_{\mathrm{cmp}} > \left| T_k + \frac{d_k}{2} \right|, k \neq n \end{cases}, \tag{17}$$

And $p_k = 1$ represents that the upper switch of phase $k$ is on and the lower switch is off; $p_k = 2$ represents that the lower switch of phase $k$ is on and the upper switch is off; $p_k = 3$ represents that the upper and lower switches of phase $k$ conduct simultaneously; and $p_k = 4$ represents that the upper and lower switches of phase $k$ are off at the same time. Since the order of each element in the matrix $G$ is that after the duty cycle ordering, it needs to be mapped to the natural phase order through reverse ordering mapping, that is

$$G_{\mathrm{nature}} = A^{-1} G. \tag{18}$$

### 2.3. The dc-link current ratio with five-phase motor drive system

The dc-link current ratio is defined as the ratio of the inverter's maximum output current amplitude to the bus current. Since the five-phase star connection is adopted, the phase current is equal to the line current, so the inverter's maximum output current amplitude is the maximum phase current amplitude.

In the case that the harmonics are zero, the motor has the five-phase symmetrical currents. From (3), the impulse duty cycles are also five-phase symmetrical duty cycles. Without affecting the results, the five-phase duty cycles can be assumed as:

$$\begin{cases} d_{\mathrm{a}} = D\cos(\theta_{\mathrm{e}}) \\ d_{\mathrm{b}} = D\cos(\theta_{\mathrm{e}} - \varphi) \\ d_{\mathrm{c}} = D\cos(\theta_{\mathrm{e}} - 2\varphi) \\ d_{\mathrm{d}} = D\cos(\theta_{\mathrm{e}} - 3\varphi) \\ d_{\mathrm{e}} = D\cos(\theta_{\mathrm{e}} - 4\varphi) \end{cases}, \tag{19}$$

where $\theta_{\mathrm{e}}$ is the electric angle, and $\varphi = 2\pi/5$. Calculate the sum of all positive duty cycles,

$$d(\theta_{\mathrm{e}}) = \frac{\sqrt{5}+1}{2} D_{\mathrm{amp}} \cos(\theta_{\mathrm{e}} - \frac{n\pi}{5}), \tag{20}$$

where $D_{\mathrm{amp}}$ is the amplitude, $\theta_{\mathrm{e}} \in [0, 2\pi]$, $n \in \{0, 1, 2, \ldots, 9\}$, and $(n - 1)\pi/10 \le \theta_{\mathrm{e}} \le (n + 1)\pi/10$.

Then the maximum sum of all positive duty cycles is $1.618D_{\mathrm{amp}}$. Since the sum of all positive duty cycles must be less than or equal to 1, the maximum value of $D_{\mathrm{amp}}$ is 0.618, and the maximum value of the output phase current is $0.618i_{\mathrm{dc}}$, that is, the dc-link current ratio is 0.618.

When the SVPWM is adopted, the 25 spatial current vectors can be divided into three groups, namely 10 large vectors with the amplitude of $1.902i_{\mathrm{dc}}$, 10 small vectors with the amplitude of $1.176i_{\mathrm{dc}}$ and 5 zero vectors. When the SVPWM with adjacent four vectors is used, the ratio of the action time between the small vector and the large vector should be 0.618 in order to make the output third harmonic be zero. Therefore, a set of middle vectors with an amplitude of $1.625i_{\mathrm{dc}}$ can be synthesized from the large vectors and small vectors. In the vector space, the tangent circle of these 10 middle vectors is taken, and its amplitude is $1.625i_{\mathrm{dc}}\cos(\pi/10) = 1.545i_{\mathrm{dc}}$. When the motor has the five-phase symmetrical currents, the amplitude of the resultant space current vector is $2.5I_{\mathrm{amp}}$, and $I_{\mathrm{amp}}$ is the amplitude of the phase current. The maximum value of the resultant space current vector is $2.5I_{\mathrm{amp}} = 1.545i_{\mathrm{dc}}$, that is, $I_{\mathrm{amp}} = 0.618i_{\mathrm{dc}}$ and the dc-link current ratio is also 0.618.

## 3. Experimental platform and control block diagram

### 3.1. Experimental platform

To verify the effectiveness of the proposed impulse modulation strategy in this paper, a five phase PMSM drive system with the current source inverter has been built as shown in Fig. 2. The experimental platform is composed of the control board, sample board, current source inverter, dc-link inductor, and five-phase PMSM. The control board selects the DSP and FPGA to execute the program, the current source inverter utilizes the IGBT as the switch and the sample board selects the LEM sensors to sample the current and voltage. And the five-phase PMSM parameters have been summarized in Table 1.

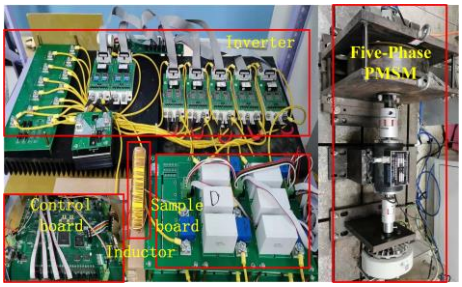


Fig. 2. Experimental platform with the current source inverter.

Table 1. Parameters of the five-phase PMSM.

| Symbol | Parameters | Value |
|---|---|---|
| $P$ | No. of pole pairs | 22 |
| $R$ | Winding resistance | 0.65 Ω |
| $L_d$ | d-axis inductance | 0.689 mH |
| $L_q$ | q-axis inductance | 0.689 mH |
| $\omega$ | Rated speed | 100 r/min |
| $T_e$ | Rated torque | 18 Nm |
| $J$ | Moment of inertia | 0.0625 kg·m$^{-2}$ |

### *3.2. Control block diagram*

The control block diagram has been shown in Fig. 3. The control system includes the *m*-phase current source inverter, *m*-phase PMSM, voltage loop, current loop, speed loop, speed calculation module, impulse modulation model, and transform models. In Fig. 3, $\theta_e$ is the electrical angle, $n_{fed}$ is the rotor speed, $n_{ref}$ is the reference of the speed controller, $i_{ref}$ is the reference of the current controller, $i_{fed}$ is the feedback of the current from the current transform module, $v_{ref}$ is the reference of the voltage controller, $v_{fed}$ is the feedback of the voltage from the voltage transform module, $v_c$ is the control value to the inverse transform module, $T_{cmp}$ is the comparison point set, $v_{sample}$ is the sample value of the *m*-phase voltage, and $i_{sample}$ is the sample value of the *m*-phase voltage, respectively.

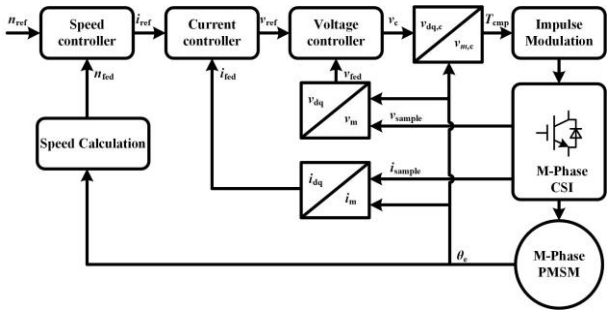


Fig. 3. Control block diagram with the *m*-phase current source inverter.

## 4. Experimental results and discussions

### *4.1. Normal operation experiment*

The system normal operation experiment results with the proposed impulse modulation strategy are shown in Fig. 4 when $T_L$ = 5 Nm, $V_{in}$ = 50 V, and $i_{dc}$ = 5 A. From Fig. 4(a), it is seen that the speed increased from 50 r/min to 100 r/min at t = 5.5 s with the ripple of 1 r/min. Fig. 4(b) shows that the motor torque increased suddenly with the maximum torque 7.0 Nm when the speed was changed. Fig. 4(c) presents the five-phase currents. When the speed was changed, the frequency of the currents increased from 18.3 Hz to 36.7 Hz. The experimental results indicate that the system can be controlled stably when the proposed impulse modulation strategy is adopted.

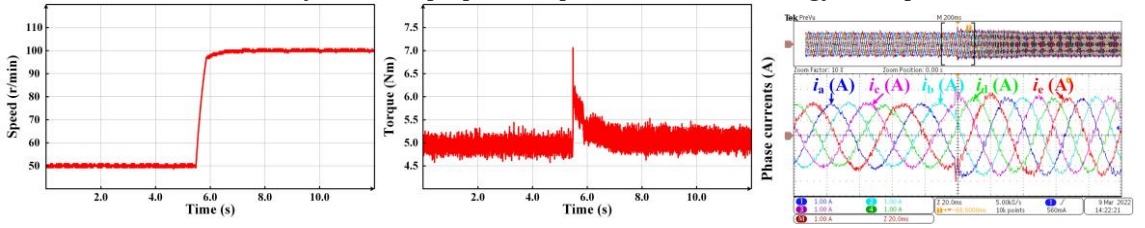


(a) (b) (c)

Fig. 4. Normal operation experiment with the impulse modulation strategy: (a) the speed; (b) the torque; and (c) the phase currents.

### *4.2. System efficiency comparison experiment*

The system efficiency comparison experimental results are shown in Fig. 5 when $V_{in}$ = 50 V, $i_{dc}$ = 5 A, $n_{ref}$ = 50 r/min, and $T_L$ = {1.0, 2.0, 3.0, 4.0, 5.0} Nm. From Fig. 5, it is seen that the system efficiency curves of the two modulation strategies are almost identical, and on the overall trend, both efficiency curves increase with the increase of the torque. When $T_L$ = 1 Nm, the system efficiencies with impulse modulation strategy and SVPWM are all about 24%, and those are about 51% when $T_L$ = 5 Nm. The experimental results indicate that the proposed impulse modulation strategy has similar performance comparing to that of the SVPWM in the aspect of system efficiency.

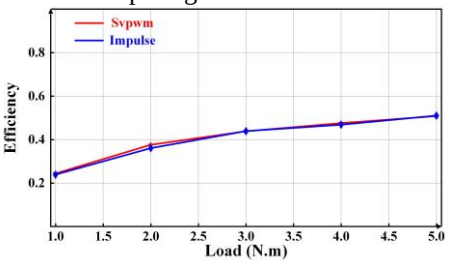


Fig. 5. System efficiency comparison with the impulse modulation strategy and SVPWM.

### *4.3. Current harmonic comparison experiment*

The current harmonic comparison experiment results are shown in Fig. 6 when $V_{in}$ = 50 V, $i_{dc}$ = 5 A, $T_L$ = 5 Nm and $n_{ref}$ = 50 r/min. When the impulse modulation strategy is used, from Fig. 6(a), it is seen that the amplitude of the fundamental waveform is about 1.4 A with the frequency 18.3 Hz, and the other harmonics are very small. When the SVPWM is used, Fig. 6(b) shows that the amplitude and frequency of the fundamental wave are the same as those of the impulse modulation strategy, and the other harmonics are also small. The experimental results show that the two modulations strategies have similar performance in the aspect of current harmonics.

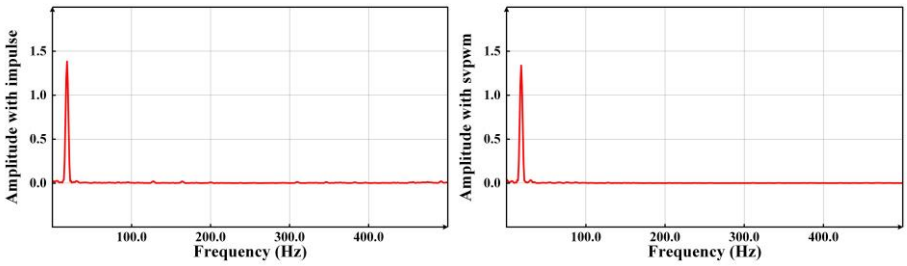


(a) (b)

Fig. 6. Current harmonics: (a) with impulse strategy; and (b) with SVPWM.

### *4.4. The dc-link current ratio experiment*

The dc-link current ratio comparison experimental results are shown in Fig. 7 when $V_{in}$ = 50 V, $i_{dc}$ = 5 A and $n_{ref}$ = 50 r/min. According to the calculation, the maximum dc-link current ratios of the impulse modulation strategy and SVPWM are all 0.618. When the impulse modulation strategy is selected, Fig. 7(a) shows that the maximum phase current amplitude can reach 3.15A with the dc-link current 5.1356 A, and hence the dc-link current ratio is 0.613, which is consistent with the theoretical calculation result. When the SVPWM strategy is adopted, Fig. 7(b) shows that the maximum phase current amplitude is also 3.15A and the dc-link current is 5.1054 A, and the dc-link current ratio is 0.617, which is almost the same as that of the impulse modulation strategy. The experimental results indicate that the two modulations have the same performance in terms of the dc-link current ratio.

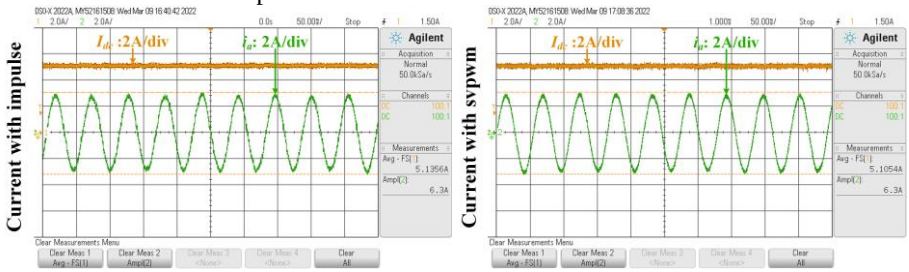


(a) (b)

Fig. 7. The dc-link current ratio: (a) the impulse modulation strategy; (b) the SVPWM strategy.

### *4.5. Dynamic response comparison experiment*

The dynamic response comparison experimental results are shown in Fig. 8 when $V_{in}$ = 50 V, $i_{dc}$ = 5 A, $n_{ref}$ = 50 r/min and $T_L$ changes from 5 Nm to 0.7 Nm. When the impulse modulation strategy is used, Fig. 8(a) shows that the speed increases by about 7 r/min after that the torque has changed from 5 Nm to 0.7 Nm as shown in Fig. 8(b). When the SVPWM is used, Figs. 8(c) and 8(d) show the speed and torque, respectively. And it can be seen that they are similar to those in Figs. 8(a) and 8(b). The experimental results indicate that the impulse strategy has similar dynamic response performance as that of SVPWM strategy.

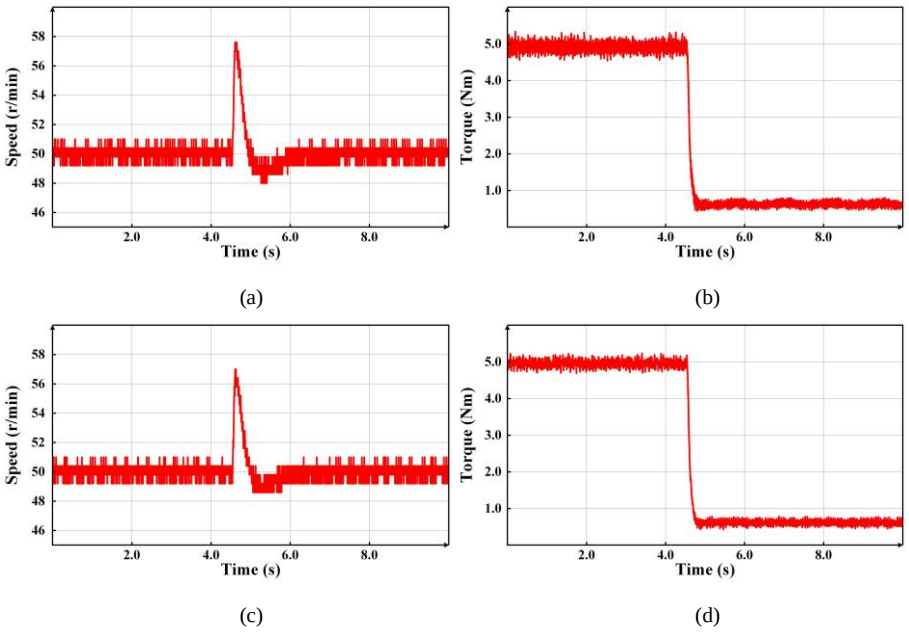


Fig. 8. Dynamic response comparison experiment: (a) the speed with the impulse modulation; (b) the torque with the impulse modulation strategy; (c) the speed with the SVPWM; (d) the torque with the SVPWM.

### *4.6. Control complexity comparison*

In the three-phase motor drive system, the SVPWM has 8 space current vectors, and the proposed impulse modulation strategy only has three impulse vectors. And in the five-phase motor drive system, the number of the space current vectors of the SVPWM is increased to 25, while the number of the impulse vectors of the impulse modulation strategy is only 5. When the SVPWM is selected, the sectors need to be calculated by the target space current vector, and then the different space current vectors are selected to design the combined strategy based on the sectors and the optimization goals. However, when the impulse modulation strategy is utilized, the combined strategy is not required, which can simplify the control complexity significantly. And when calculating the dwell time of the space current vectors, the SVPWM needs different calculation equations when the sector is different, leading to the complex calculation. While the impulse modulation strategy can calculate the dwell time with the same equation. Furthermore, when generating the PWM wave, the SVPWM needs to combine the sector, the selected space current vectors and the dwell time, which is complex, but the impulse modulation strategy only needs the dwell time and the impulse vectors, which can simplify the process. Above all, the proposed modulation strategy has lower control complexity than the SVPWM, and the advantages are even more pronounced when it is extended to the multi-phase motor drive system.

Table 2. Control complexity comparison.

| Item | Impulse modulation strategy | SVPWM |
|---|---|---|
| Quantity of the control vectors of *m*-phase motor | $m$ | $m^2$ |
| Combined strategy | No combined strategy is required and all impulse vectors are involved. | Based on the different sectors and optimization objectives, different current vectors are selected to design the combined |

| | | |
|---|---|---|
| | | strategy. |
| Dwell time | The same calculation equations are used. | Different equations are required when the sector is different. |
| PWM generation | Based on the dwell time and the impulse vectors. | Based on the sector, the selected space current vectors and the dwell time. |

## 5. Conclusion

In this paper, a novel impulse modulation strategy for PMSM with current source inverter is proposed to reduce the complexity of the traditional SVPWM strategy. The key novelties are as follows:

1. At an m-phase motor drive system, the proposed method requires m current impulses to control the system, compared to that the SVPWM needs $m^2$ space current vectors.

2. This method does not select the sector, and the calculation of the comparison points and the generation of the PWM can be achieved without the change of the equations. In comparison, the SVPWM needs to select different space current vectors to calculate the comparison points and generate the PWM by different sector.

3. Compared to the SVPWM, this method has similar performance in the aspects of the efficiency, output current harmonic, and dc-link current ratio and dynamic response.

This method is easy to implement and can be easily extended to multi-phase current source inverter. The future research direction is to study the application of the modulation strategy and the control strategy based on the impulse strategy.

## References

[1] L. Qu, W. Qiao, L. Qu. An extended-state-observer-based sliding-mode speed control for permanent-magnet synchronous motors. *IEEE J. Emerg. Sel. Topics Power Electron.* 2021;**9(2)**:1605-1613.

[2] W. Xu, A. K. Junejo, Y. Liu, M. R. Islam. Improved continuous fast terminal sliding mode control with extended state observer for speed regulation of PMSM drive system. *IEEE Trans. Veh. Technol*. 2019;**68(11)**:10465-10476.

[3] F. F. M. El-Sousy, M. M. Amin, O. A. Mohammed. Robust optimal control of high-speed permanent-magnet synchronous motor drives via self-constructing fuzzy wavelet neural network. *IEEE Trans. Ind. Appl.* 2021;**57(1)**:999-1013.

[4] S. K. Kim, J. S. Lee, K. B. Lee. Self-tuning adaptive speed controller for permanent magnet synchronous motor. *IEEE Trans. Power Electron.* 2017;**32(2)**:1493-1506.

[5] H. Chaoui, M. Khayamy, O. Okoye, H. Gualous. Simplified speed control of permanent magnet synchronous motors using genetic algorithms. *IEEE Trans. Power Electron.* 2019;**34(4)**:3563-3574.

[6] L. N. Tan, T. P. Cong, D. P. Cong. Neural network observers and sensorless robust optimal control for partially unknown PMSM with disturbances and saturating voltages. *IEEE Trans. Power Electron.* 2021;**36(10)**:12045-12056.

[7] S. K. Kim, C. K. Ahn. Offset-free proportional-type self-tuning speed controller for permanent magnet synchronous motors. *IEEE Trans. Ind. Electron.* 2019;**66(9)**:7168-7176.

[8] Y. Xu, Z. Wang, P. Liu, J. He. A soft-switching current-source-inverter-fed motor drive with reduced common-mode voltage. *IEEE Trans. Ind. Electron.* 2021;**68(4)**:3012-3021.

[9] G. Migliazza, et al. DC current control for a single-stage current source inverter in motor drive application. *IEEE Trans. Power Electron.* 2021;**36(3)**:3367-3376.

[10] J. D. Ma, B. Wu, N. R. Zargari, S. C. Rizzo. A space vector modulated CSI-based AC drive for multimotor applications. *IEEE Trans. Power Electron.* 2001;**16(4)**:535-544.

[11] J. I. Guzmán, J. R. Espinoza, L. A. Morán, G. Joós. Selective harmonic elimination in multimodule three-phase current-source converters. *IEEE Trans. Power Electron.* 2010;**25(1)**:44-53.

[12] G. S. Kulothungan, A. Edpuganti, A. K. Rathore, J. Rodriguez, D. Srinivasan. Hybrid SVM-SOPWM modulation of current-fed three-level inverter for high power application. *IEEE Trans. Ind. Appl.* 2019;**55(4)**:4344-4358.

[13] X. Guo, D. Xu, B. Wu. Common-mode voltage mitigation for back-to-back current-source converter with optimal space-vector modulation. *IEEE Trans. Power Electron.* 2016;**31(1)**:688-697.

[14] A. Hu, D. Xu, B. Wu, J. Wang, J. Su. Reference-trajectory-optimized SVM for high-power current-source converters to improve harmonic performance and reduce common-mode voltage. *IEEE Trans. Power Electron.* 2015;**30(7)**:3488-3498.
[15] X. Guo, D. Xu, B. Wu. Four-leg current-source inverter with a new space vector modulation for common-mode voltage suppression. *IEEE Trans. Ind. Electron.* 2015;**62(10)**:6003-6007.
[16] J. Shang, Y. W. Li, N. R. Zargari, Z. Cheng. PWM strategies for common-mode voltage reduction in current source drives. *IEEE Trans. Power Electron.* 2014;**29(10)**:5431-5445.
[17] J. Shang, Y. W. Li. A space-vector modulation method for common-mode voltage reduction in current-source converters. *IEEE Trans. Power Electron.* 2014;**29(1)**:374-385.
[18] Y. Lian, Y. Zhang, Y. W. Li, N. R. Zargari, Z. Cheng. Common-mode resonance suppression in transformerless PWM current-source drive. *IEEE Trans. Power Electron.* 2016;**31(8)**:5721-5731.
[19] H. Gao, B. Wu, D. Xu, M. Pande, R. P. Aguilera. Common-mode-voltage-reduced model-predictive control scheme for current-source-converter-fed induction motor drives. *IEEE Trans. Power Electron.* 2017;**32(6)**:4891-4904.
[20] Y. Lian, Y. W. Li, Z. Quan, N. R. Zargari, Z. Cheng. SVM strategies for common-mode current reduction in transformerless current-source drives at low modulation index. *IEEE Trans. Power Electron.* 2017;**32(2)**:1312-1323.
[21] E. Lorenzani, F. Immovilli, G. Migliazza, M. Frigieri, C. Bianchini, M. Davoli. CSI7: a modified three-phase current-source inverter for modular photovoltaic applications. *IEEE Trans. Ind. Electron.* 2017;**64(7)**:5449-5459.
[22] Z. Wang, B. Wu, D. Xu, N. R. Zargari. Hybrid PWM for high-power current-source-inverter-fed drives with low switching frequency. *IEEE Trans. Power Electron.* 2011;**26(6)**:1754-1764.
[23] A. N. Ghule, P. Killeen, D. C. Ludois. Synchronous electrostatic machine torque modulation via complex vector voltage control with a current source inverter. *IEEE J. Emerg. Sel. Topics Power Electron.* 2020;**8(2)**:1850-1857.
[24] P. Liu, Z. Wang, Q. Song, Y. Xu, M. Cheng. Optimized SVM and remedial control strategy for cascaded current-source-converters-based dual three-phase PMSM drives system. *IEEE Trans. Power Electron.* 2020;**35(6)**:6153-6164.
[25] X. Guo, Y. Yang, X. Wang. Optimal space vector modulation of current-source converter for DC-link current ripple reduction. *IEEE Trans. Ind. Electron.* 2019;**66(3)**:1671-1680.
[26] X. Guo, D. Xu, J. M. Guerrero, B. Wu. Space vector modulation for DC-link current ripple reduction in back-to-back current-source converters for microgrid applications. *IEEE Trans. Ind. Electron.* 2015;**62(10)**:6008-6013.
[27] Y. Zhang, Y. W. Li. Investigation and suppression of harmonics interaction in high-power PWM current-source motor drives. *IEEE Trans. Power Electron.* 2015;**30(2)**:668-679.
[28] W. Wang, F. Gao, Y. Yang, F. Blaabjerg. An eight-switch five-level current source inverter. *IEEE Trans. Power Electron.* 2019;**34(9)**:8389-8404.
[29] Y. Geng, R. Deng, W. Dong, K. Wang, H. Liu, X. Wu. An overlap-time compensation method for current-source space-vector PWM inverters. *IEEE Trans. Power Electron.* 2018;**33(4)**:3192-3203.
[30] A. Singh, J. Benzaquen, B. Mirafzal. Current source generator–converter topology for direct-drive wind turbines. *IEEE Trans. Ind. Appl.* 2018;**54(2)**:1663-1670.
[31] X. Guo. Three-phase CH7 inverter with a new space vector modulation to reduce leakage current for transformerless photovoltaic systems. *IEEE J. Emerg. Sel. Topics Power Electron.* 2017;**5(2)**:708-712.
[32] S. Anand, S. K. Gundlapalli, B. G. Fernandes. Transformer-less grid feeding current source inverter for solar photovoltaic system. *IEEE Trans. Ind. Electron.* 2014;**61(10)**:5334-5344.